Journal of NeuroVirology, 7: 105–116, 2001
© 2001 Taylor & Francis ISSN 1355–0284/01 $12.00+.00

Differences in pathogenicity of herpes simplex virus serotypes 1 and 2 may be observed by histopathology and high-resolution magnetic resonance imaging in a murine encephalitis model

Heath C Thomas,[1] Rasesh D Kapadia,[2] Grace I Wells,[3] Andrew M Gresham,[3] David Sutton,[3] Henk A Solleveld,[1] Susanta K Sarkar,[2] Susan B Dillon,[3] and Ruth Tal-Singer[3]

Departments of [1]Safety Assessment, [2]Physical and Structural Chemistry, and [3]Molecular Virology and Host Defense, at SmithKline Beecham Pharmaceuticals, Collegeville, Pennsylvania, USA

The mouse model for herpes simplex-induced encephalitis (HSE) is an established preclinical tool for evaluating the efficacy of new therapeutic interventions. We evaluated the utility of high-resolution *in vivo* MRI in observing the progression of experimental HSE during the first week postinfection. Female BALB/c mice were inoculated intracerebrally with HSV-1 or HSV-2 by microinjection. Each animal was evaluated daily by high-resolution (4.7 Tesla) T_2 weighted MRI and clinical disease scoring (neurological and behavioral). Lesions induced by a high dose of HSV-1 (1000 PFU) were detectable by MRI without administration of contrast agent whereas for low dose HSV-1 (100 PFU), administration of contrast agent was necessary to visualize the lesions in the brain. The correlation between the MRI and histologic results was excellent. No HSV-2 induced lesions were observed by MRI. Although both HSV serotypes caused similar clinical disease, significant type differences were found by histologic and MRI examinations. HSV-1 caused necrotizing meningoencephalitis, whereas HSV-2 induced mostly meningitis. The data indicate that *in vivo* high-resolution MRI may be useful to longitudinally evaluate HSV-1-related pathology in a mouse model of HSE and potentially could be used for monitoring the efficacy of anti-infective therapeutic approaches. *Journal of NeuroVirology* (2001) **7,** 105–116.

Keywords: HSV; encephalitis; MRI; mouse; histopathology

Introduction

Herpes simplex encephalitis (HSE) is a severe sporadic disease that accounts for 10–20% of viral encephalitis cases. In many cases, infection causes focal, necrotizing lesions that result in severe neurological sequelae. As such, HSE is the most severe form of herpes simplex virus (HSV) infection (Nahmias *et al*, 1982; Corey and Spear, 1986; Whitley *et al*, 1998). Both HSV-1 and HSV-2 have been associated with infections of the central nervous system (CNS). In neonates or immunocompromised individuals, HSV-2 can cause fatal encephalitis. In contrast, HSV-2 infections in immunocompetent individuals result in myelitis and mild meningitis (Craig and Nahmias, 1973; Nahmias *et al*, 1982; Bergstrom *et al*, 1990). HSV-1 is the most common cause of necrotizing HSE in patients over 3 months of age (Whitley and Lakeman, 1995; Skoldenberg, 1996; Levitz, 1998) and results in at least 70% mortality and severe morbidity in survivors. Antiviral treatment may reduce HSE-associated mortality rate to approximately 30%, but may still leave survivors with severe neurological impairment (Whitley and Lakeman, 1995; Skoldenberg, 1996). Thus, improvements in HSE therapy are still important research goals.

Magnetic resonance imaging (MRI) is a useful clinical diagnostic technique for following the progress of acute HSE in humans (Whitley and Lakeman,

Address correspondence to R Tal-Singer, SmithKline Beecham Pharmaceuticals, 1250 S. Collegeville Road, P.O. Box 5089, Collegeville, PA 19426, USA. E-mail: Ruth_Tal-Singer-1@sbphrd.com
Received 24 February 2000; revised 13 July 2000; accepted 19 October 2000

1995). The utility of MRI for following morphological changes in murine brains after intranasal inoculation with HSV-1 strain F was recently demonstrated (Meyding-Lamade *et al*, 1998a, 1999). However, a systematic comparison of high-resolution MR images to histologically identified lesions produced by HSV infection was never conducted and was therefore the rationale for this study. We followed the pathogenesis of HSV-1 (strain SC-16) and HSV-2 (strain SB-5) in a mouse model of HSE by comparing clinical disease, and histopathology end points with high-resolution MRI.

Several murine models for HSE have been described (Anderson and Field, 1983). Although intranasal inoculation mimics acquisition of HSE from the periphery, infections with HSV-1 or HSV-2 can lead to viremia and infection in other organs such as the lung and liver (Kern *et al*, 1982). Neuroinvasiveness is dependent in part on the ability of the virus to replicate in the periphery and spread to the CNS (Oakes *et al*, 1986; Day *et al*, 1988; Yeung *et al*, 1991). Therefore, we chose the intracerebral inoculation model for a direct comparison of HSV-1 and HSV-2 induced pathogenesis in the CNS.

Results

Pathology observed by MRI correlates to histopathology results

Mice were inoculated intracerebrally with 100 ($n = 5$) or 1000 ($n = 5$) PFU of HSV-1 (SC-16), then monitored daily using MRI for up to 7 days. All mice were prescanned prior to infection to establish a baseline. The mice demonstrated clinical symptoms of CNS disease, including ruffled coats, hunched posture, and poor response to stimuli. Most mice showed severe morbidity by day 4 postinfection, and 3/5 and 4/5 mice infected with 100 or 1000 PFU, respectively, were moribund by day 5. Daily MRI scans were obtained from all animals up to day 4 and two surviving animals infected with 100 PFU were scanned on day 7.

Animals inoculated with 1000 PFU A series of representative MR images (three 1-mm slices) from one mouse, before and after infection with 1000 PFU of HSV-1 (SC-16) are shown in Figure 1. A region of high signal intensity (hyperintensity), indicating inflammatory cell infiltration, can be visualized as early as day 2 following infection. The hyperintense regions increase in size and intensity with time, as is shown by arrows on the images from day 4 following infection when the animal demonstrated severe clinical signs (clinical score = 10).

On day 4 postinfection, prior to histologic evaluation, *ex vivo* MR images of formalin-fixed brains were collected at 9.4 T. The images shown in Figure 2 demonstrate the excellent anatomical resolution obtained by this method, as well as the correlation between MR pathology and the localization of viral antigen. In Panel A, 1-mm sagittal sections from rostral cerebrum, cerebellum, and brain stem MR images show regions of hyperintensity (white) surrounding the fornix and corpus callosum, as well as the lateral ventricle outlining a central area of hypointensity (black). The left lateral ventricle appears dilated. In Panel B, frequent HSV-1 antigen-positive cells (antigen score = 3) were present within the cerebral cortex, thalamus, hypothalamus, and within the cerebellar brain stem in corresponding paraffin embedded sections. Note the linear strip of antigen staining in the cerebral cortex, and the foci of intense staining in the anterior hypothalamus (Panel B, top image). There are small foci of antigen-positive cells in the cerebellar molecular layer, as well as the subadjacent brain stem (Panel B, bottom image). The correlation between MR and antigen staining is particularly evident in a locally extensive region surrounding the corpus callosum and fornix, and around the left lateral ventricle (Panels A and B, top images). Histologic alterations observed in H&E stained sections consisted of severe extensive necrotizing meningoependymoencephalitis (pathology score = 16), as well as eosinophilic intranuclear inclusion bodies (data not shown) within the same areas that were antigen- and/or MR pathology-positive (Figures 1 and 2).

Animals inoculated with 100 PFU *In vivo* MRI studies of mice infected with 100 PFU of HSV-1 did not show clear hyperintense regions within the brain and required administration of intravenous contrast agent to better observe inflammatory changes. This is consistent with findings in a study using 1.5 T MRI in a different infection model (Meyding-Lamade *et al*, 1998b). The reduction in MR pathology following lower viral inoculum was mirrored by reduced expression of antigen, and reduced lesion severity detected by H&E histology (not shown). In contrast to lesion severity, the anatomical localization of lesions was similar in all animals infected with either 100 or 1000 PFU. In Figure 3, an *in vivo* 4.7 T MR image from Mouse B-6 (Table 2) demonstrates a possible hyperintensity in the region of the dentate gyrus and hippocampus (Panel A). However, an image obtained from the same mouse following injection of contrast agent helps identify the hyperintense region within the hippocampus and cerebral cortex

Table 1 Histopathology scoring system

Meningitis[a]	*Encephalitis*[a]	*Lateral Ventricular Dilation*
absent = 0	absent = 0	absent = 0
minimal = 1	minimal = 1	minimal = 1
mild = 2	mild = 2	mild = 2
moderate = 3	moderate = 3	moderate = 3
severe = 4	severe = 4	severe = 4

[a]For the categories of meningitis and encephalitis, if necrosis was present the individual score was doubled. The scores for each of the individual categories were then added together to arrive at the final pathology score for the animal.

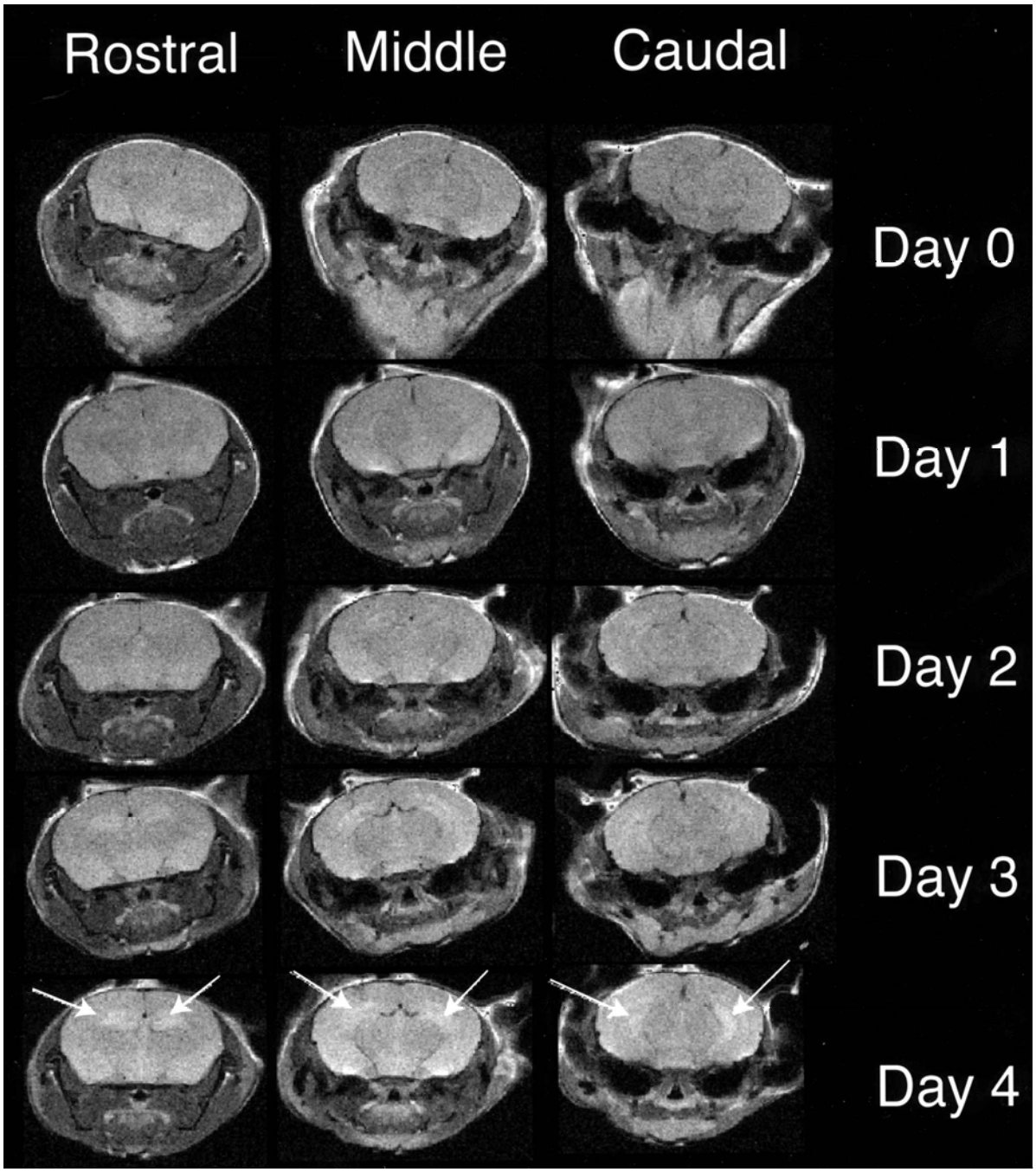

Figure 1 Daily 4.7 Tesla MRI demonstrates progression of HSV-1-induced damage. A BALB/c mouse was infected with 1000 PFU of HSV-1 (SC-16). On days 0, 1, 2, 3, and 4 it was anesthetized and subjected to 15 min of 4.7 T magnetic resonance imaging. Each daily panel contains 3 representative 1-mm sagittal sections out of a total of 12. Arrows denote hyperintense regions.

(Figure 3, Panel B, arrows). Moreover, imaging with contrast agent revealed a high-intensity region seen in the area of the 3rd ventricle (Panel B, base of skull), which possibly represents the breakdown of the blood–brain barrier due to damage to the ependymal cell layer (Kesari *et al*, 1998). Immunostaining for HSV-1 antigen in corresponding sections demonstrated strong positive antigen staining in the left dentate gyrus and hippocampus, as well as the right lower cerebral cortex also seen by contrast enhanced MR pathology (Panel C). Consistent with the presence of contrast agent in the ventricles, immunostaining and histopathology analysis at high-power magnification demonstrated numerous antigen-positive cells in meningeal and ependymal cells, as well as necrotizing meningitis (data not shown). Thus, the introduction of contrast agent greatly enhances the sensitivity of detection. For subsequent studies, we

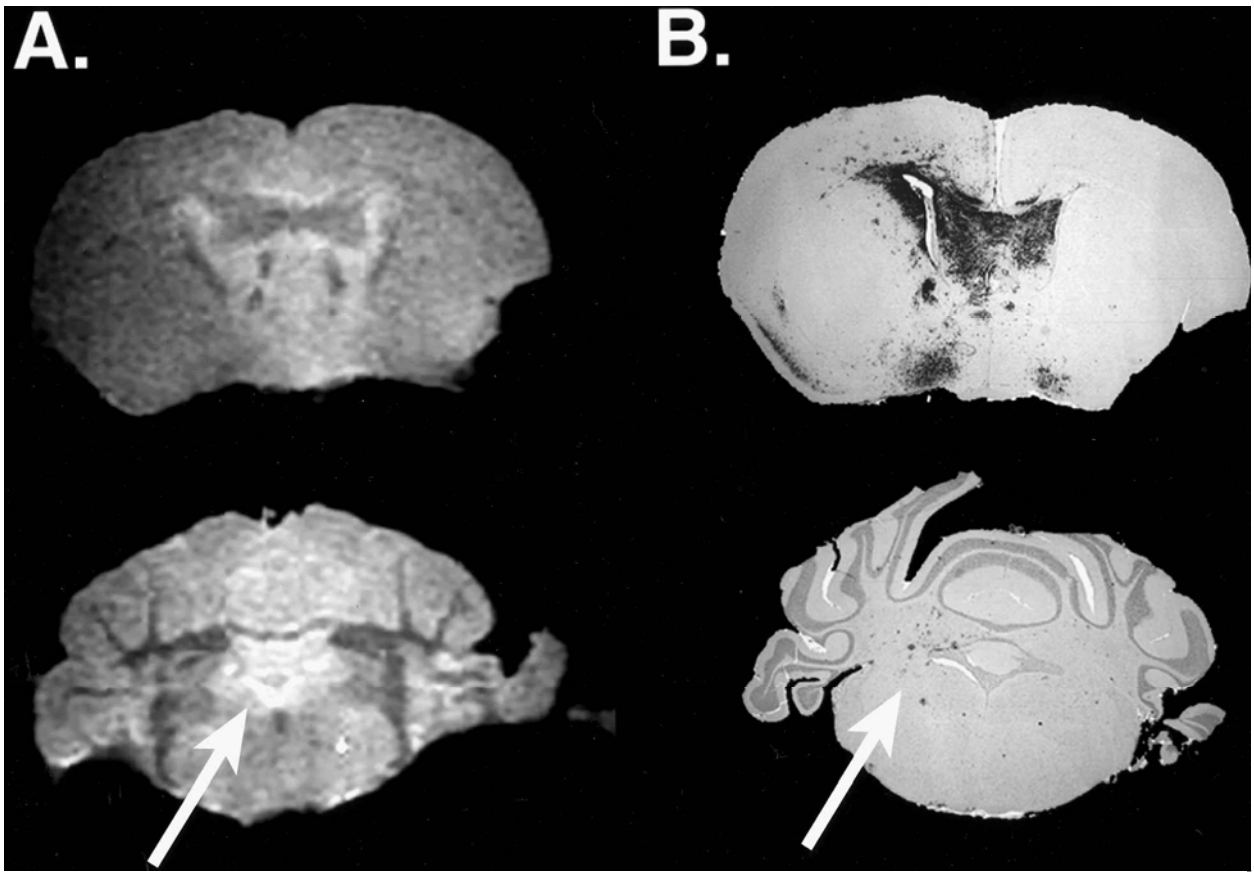

Figure 2 High-resolution MRI lesions correlate with HSV-1 antigen expression. The mouse described in the legend of Figure 1 was euthanized on day 4 postinfection, its brain was removed then fixed in formalin. (**A**) 1-mm sagittal 9.4 T MR sections from the rostral cerebrum, cerebellum, and brain stem. (**B**) Corresponding paraffin sections stained for HSV-1 antigen. Magnification 8X.

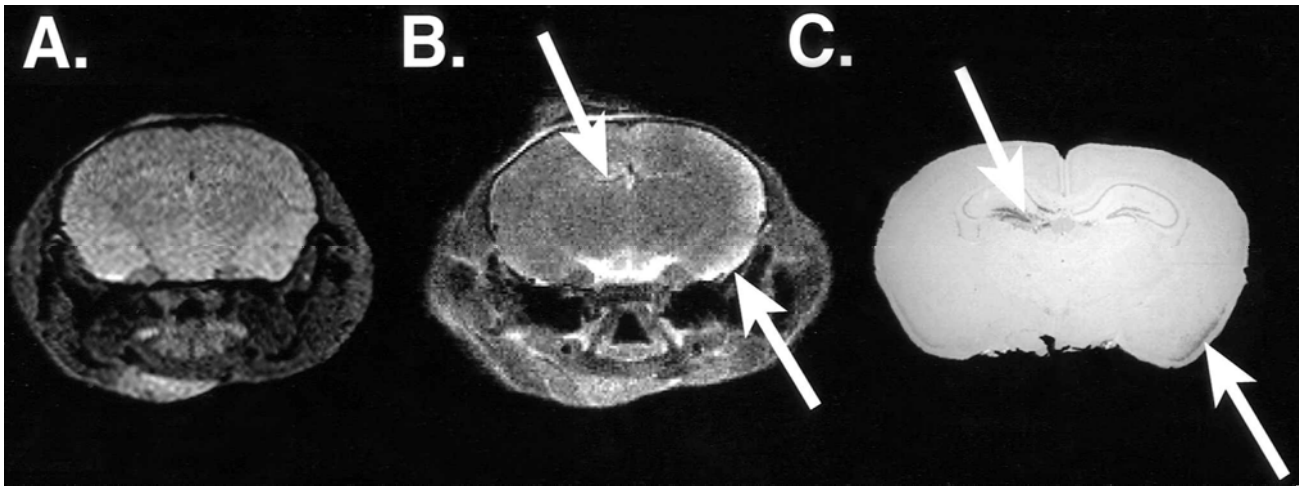

Figure 3 Monitoring of low dose (100 PFU) of HSV-1-induced lesions by administration of contrast agent. On day 4 postinfection, mouse B-6 (Table 2) was subjected to *in vivo* 4.7 T MRI without, then with contrast. Brain was then collected and processed for histologic evaluation. (**A**) A 1-mm image in the absence of contrast agent. (**B**) An *in vivo* 4.7 T MR slice following intravenous injection of contrast agent. Arrows point to pathological lesions within the left dentate gyrus and hippocampus, as well as the right lower cerebral cortex. (**C**) An immunostain of a corresponding paraffin section. The arrows indicate HSV-1 antigen-positive areas corresponding to those shown in **B** (magnification 8X).

Table 2 Comparison of HSV-1 and HSV-2 pathogenesis in BALB/c mice

Virus	*Day*[a]	*Animal*	*Clinical score*[b]	*Antigen HSV1/2*[b]	*Pathology score*[b]	*MR Lesion*[c]
None		Mock	0	0/0	0	n
HSV-1	2	B-1	6.5	1/1	6	y
HSV-1	2	B-2	6.5	1/1	8	y
HSV-1	2	B-3	6.5	1/1	8	n
HSV-1	2	B-4	6.5	1/1	6	y
HSV-1	2	B-5	6.5	2/1	6	n
HSV-1	4	B-6	10	2/2	10	y
HSV-1	4	B-7	9.5	3/3	14	y
HSV-1	4	B-8	8.5	2/2	5	y
HSV-1	4	B-9	10	ND	ND	y
HSV-2	2	B-10	5.5	0/1	1	n
HSV-2	2	B-11	5.5	1/1	14	y
HSV-2	2	B-12	5.5	1/1	4	n
HSV-2	2	B-13	10	ND	ND	n
HSV-2	2	B-14	5.5	0/1	4	n
HSV-2	2	B-15	5.5	0/1	4	n
HSV-2	4	B-16	10	1/1	1	n
HSV-2	4	B-17	8.5	1/1	2	n
HSV-2	4	B-19	8.5	0/1	6	n

[a]Sampling day following infection with 100 PFU HSV-1 or HSV-2.
[b]Clinical, antigen, or histopathology scores based on criteria defined in Materials and methods.
[c]The presence of MR lesion in any of the sections collected on sampling day using 4.7 T imaging.

chose an inoculum titer of 100 PFU per brain to improve survival through day 4, all MR scans were performed first without then with contrast agent.

Pathology is not due to intracerebral inoculation

To determine whether the lesions observed by MRI and histology resulted from infection and not brain trauma, we compared mock-infected with HSV-infected animals (100 PFU/brain, $n = 5$) using MRI, immunostaining, and histopathology. MRI demonstrated pathology only in infected animals with similar distribution of lesions among all animals scanned (data not shown). As expected, samples from mock-infected animals were negative for HSV-1 antigen, had focal areas of hemorrhage within the brain parenchyma at the site of injection, and occasionally accumulations of red blood cells within the lateral ventricular system. As observed before, HSV-1 infected sections had widespread antigen-positive cells throughout the cerebral cortex, thalamus region, cerebellar brain stem, cerebellar molecular and Purkinje cell layers, and scattered antigen-positive foci within the meninges. Histologically, there was corresponding locally extensive severe necrotizing encephalitis, in addition to mild multifocal necrotizing meningitis within the regions that were antigen and MRI lesion positive (data not shown). Thus, we conclude that the pathology observed by MR was induced by HSV-1 infection and not due to brain trauma induced by injection.

HSV-1 (SC-16) and HSV-2 (SB-5) induce different brain pathology

Clinical disease and pathology were evaluated in mice inoculated with 100 PFU of HSV-1 (SC-16) or HSV-2 (SB-5). Both serotypes caused severe, clinical neurological disease as summarized in Table 2. Similar to our previous observations using this inoculum, severe pathology was observed by MR in most HSV-1 infected animals (Table 2). Some variability was observed in intensity and size of pathological changes, possibly due to interanimal variability. Features seen in MR images from different animals in this experiment included dispersed hyperintensity in various brain structures, hyperintense striations in the cerebral cortex, and ventricular enlargement. In mice infected with HSV-1, HSV antigen-positive cells were common and tended to be diffusely disseminated throughout the brain. Strong positive staining was typically present within regions of the hippocampus (Figure 4, Panel A), cerebrum, brain stem, and meninges (Figure 4, Panel C). The associated histologic lesions were characterized as minimal to severe necrotizing meningoencephalitis affecting the brain stem, hippocampal regions, and cerebrum along with the cerebellum (not shown). Eosinophilic intranuclear inclusion bodies were sometimes present within lesions (Figure 4, Panel E). Dilation of the ventricular system was observed in most samples. Infrequent HSV-1 antigen-positive cells were also observed within the spinal cord or the meninges of the spinal cord and were associated with histological evidence of mild meningitis (data not shown).

Pathology due to HSV-2 infection could not be visualized by *in vivo* MR imaging of most animals infected with 100 PFU even in the presence of severe clinical disease (Table 2, B-13, B-16, B-17, B-19). This was consistent with the limited meningeal histopathology observed in H&E stained sections. In contrast to mice

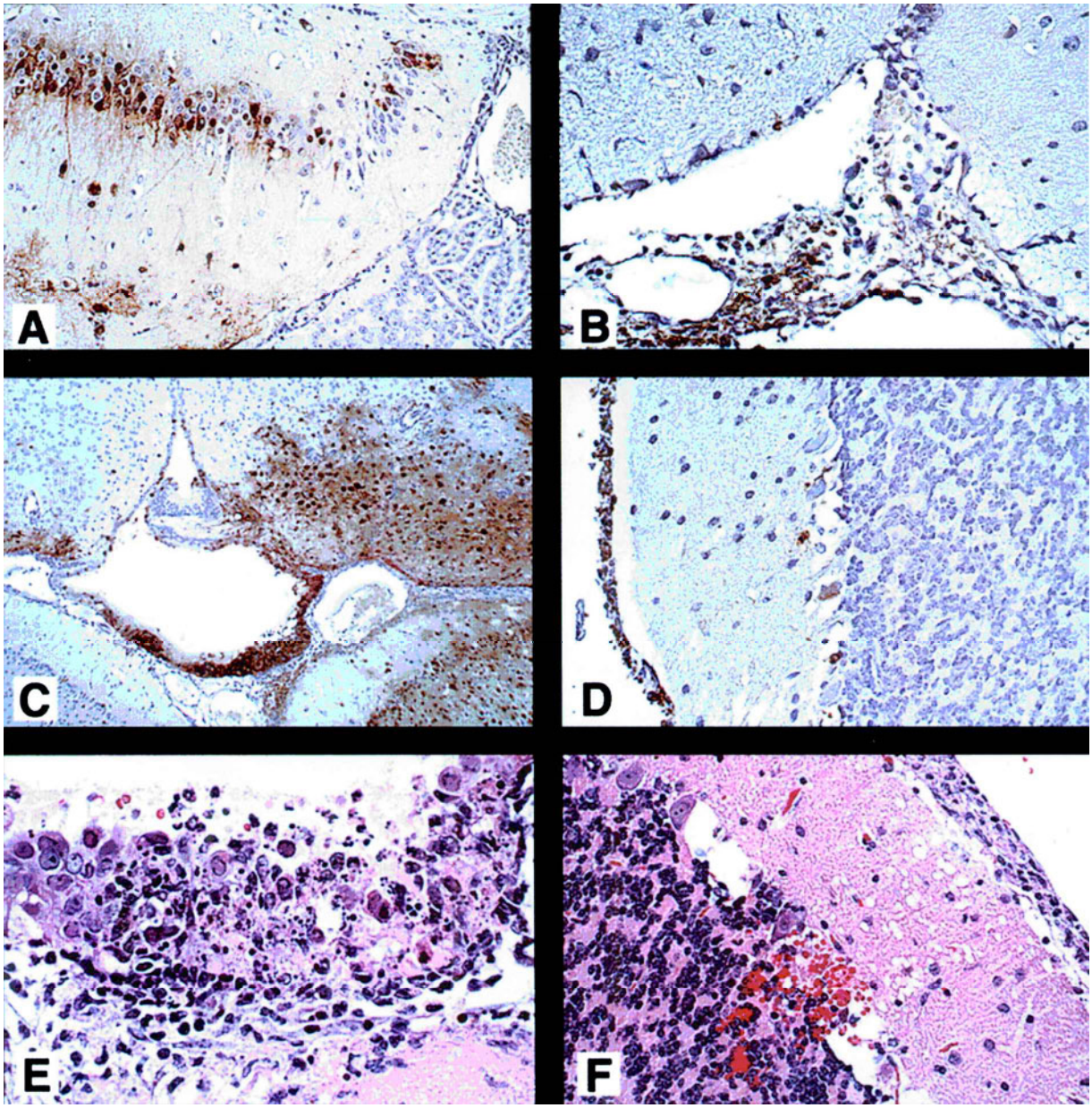

Figure 4 Differences between HSV serotypes correlate with antigen distribution and histopathology. Mice were infected intracranially with 100 PFU of HSV-1 or HSV-2. Disease was evaluated in individual animals (summarized in Table 2). (**A**), (**C**), and (**E**) correspond to animals infected with HSV-1; (**B**), (**D**), and (**F**) correspond to animals infected with HSV-2. (**A**) (magnification 108X): Immunostain of a brain section from the animal presented in Figure 3 (mouse B-6). Shown is intense antigen staining (brown) within neuronal cell bodies, axons, and dendrites of the left dentate gyrus. (**B**) (magnification 215X): Numerous inflammatory and meningeal cells strongly express HSV antigen within the thickened meninges (mouse B-17). (**C**) (magnification 55X): Antigen-positive cells within the ependyma and choroid plexus cells lining the third ventricle, as well as most neurons and supporting cells within the surrounding parenchyma (mouse B-7). (**D**) (magnification 215X): Thickened meninges and antigen-positive cells within the molecular layer of the underlying cerebellar folia (mouse B-4). (**E**) (magnification 325X): High magnification of an H&E stained serial section of the ependymal region shown above in (**C**) (mouse B-7). Marked necrosis, inflammation and several eosinophilic intranuclear viral inclusion bodies are apparent. (**F**) (magnification 215X): An H&E stained section of the cerebellum obtained from the brain shown in (**B**) (mouse B-17). Thickened inflamed meninges with subadjacent vacuolation of the molecular layer, and focal hemorrhage within the granular layer are present. This meningeal pathology with occasional invasion into the underlying parenchyma was typical of HSV-2 infected samples.

infected with HSV-1, dilation of the ventricular system was rarely present following infection with HSV-2 (SB-5). It is of interest to point out that changes in MR images were observed in a single HSV-2 infected mouse with relatively lower clinical score (5.5) following injection of contrast agent (Table 2, animal B-11). Histologic lesions in brain sections obtained from this mouse consisted of necrotizing meningitis with extension into the subadjacent parenchyma and necrotizing encephalitis.

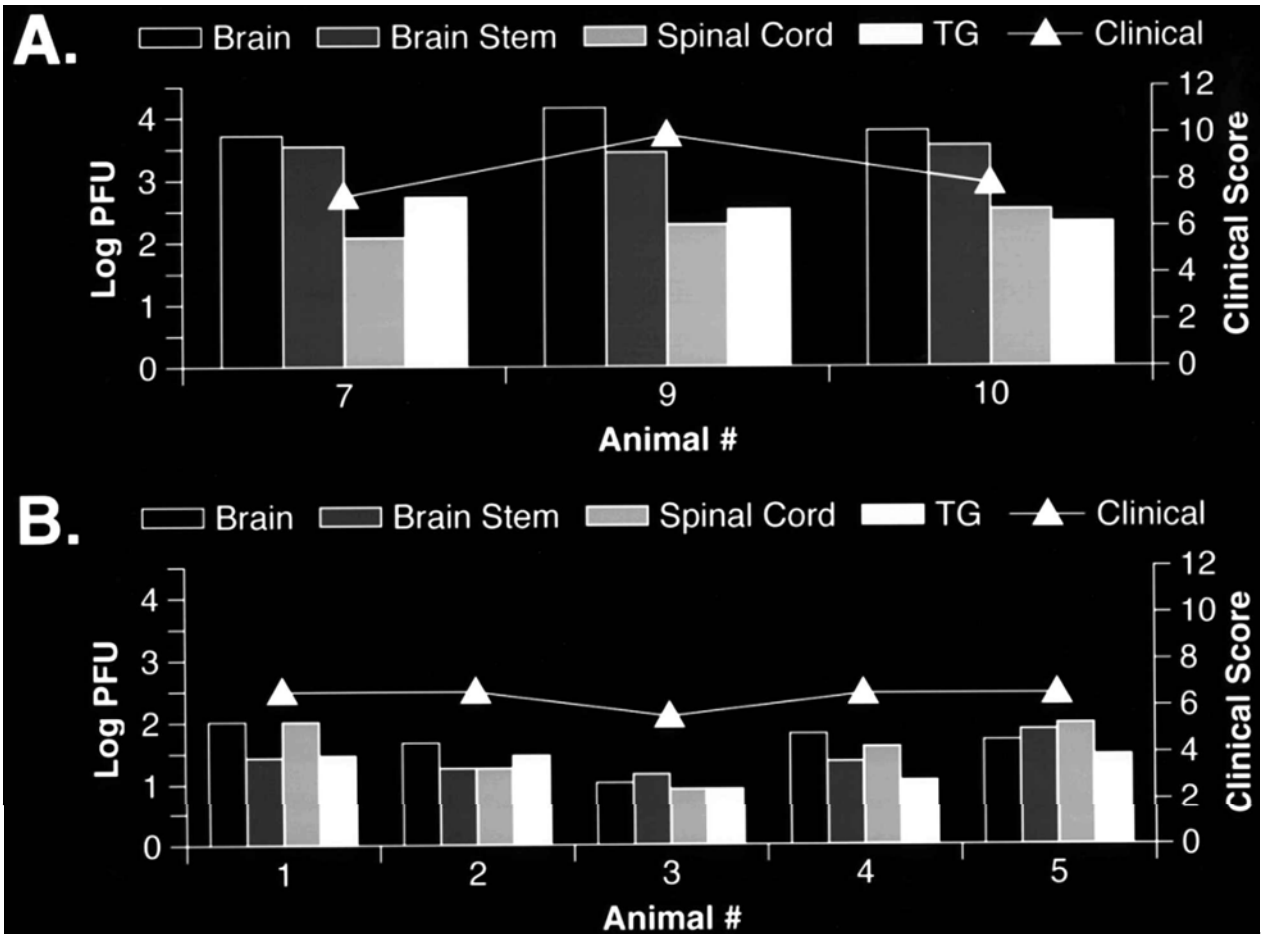

Figure 5 Differences between HSV-1 and HSV-2 titers are evident on day 4. BALB/c mice were infected with 100 PFU of HSV-1 (SC-16) or HSV-2 (SB-5). On day 4 following infection clinical scores were determined (line, right axis) and multiple tissues were removed for determination of virus titers (bars, left axis). (**A**) Three survivors of HSV-1 infection. (**B**) Five HSV-2-infected mice. No virus was detected in livers, spleens, hearts, lungs, or kidneys.

In most brain sections obtained from HSV-2 infected mice, HSV-antigen staining was confined to the meningeal and ventricular system regions along with associated infiltrating inflammatory cells. Antigen-positive cells could only be visualized by high power magnification (Figure 4, Panels B and D). Some animals infected with HSV-2 had focal areas of viral invasion into the underlying parenchyma, typically within the cerebellum, as can be seen in Figure 4, Panel D. Histologic lesions in those foci consisted of minimal malacia and hemorrhage, as well as eosinophilic nuclear inclusions (Figure 4, Panel F). In some animals, individual antigen-positive neurons were observed occasionally within the cerebral cortex, hippocampus, and brain stem. Infrequent HSV antigen-positive meningeal cells surrounding the spinal cord were also present.

To determine whether MRI and histologic differences between HSV serotype were inoculum titer-dependent, we evaluated mice infected with 1000 PFU of HSV-2. Again, we were unable to definitively identify histologically identified meningeal lesions by MRI (data not shown). Moreover, there was an increase in antigen-positive cells detected in the parenchyma subadjacent to the meninges and ventricular systems, but antigen distribution within the brain was similar to that detected in mice infected with 100 PFU. We concluded that even at higher titers, HSV-2 induced MR pathology, inflammatory changes, and antigen distribution appear different from HSV-1.

HSV-2 (SB-5) replication is restricted to the CNS

To determine whether the differences in pathology are due to differences in virus spread or replication, animals were infected with 100 PFU of each virus strain. Brain, brain stem, spinal cord, liver, spleen, heart, lung, trigeminal ganglia (TG), kidney, skeletal muscle and cervical lymph node were analyzed for viral load in samples obtained on day 4 postinfection. As shown in Figure 5, both HSV serotypes caused severe clinical disease. However, HSV-2 titers were 1–2 logs lower than HSV-1 in brain, brain stem, TG, and spinal cord titers. No virus was detected in other tissues, in agreement with the lack of antigen staining (data not shown).

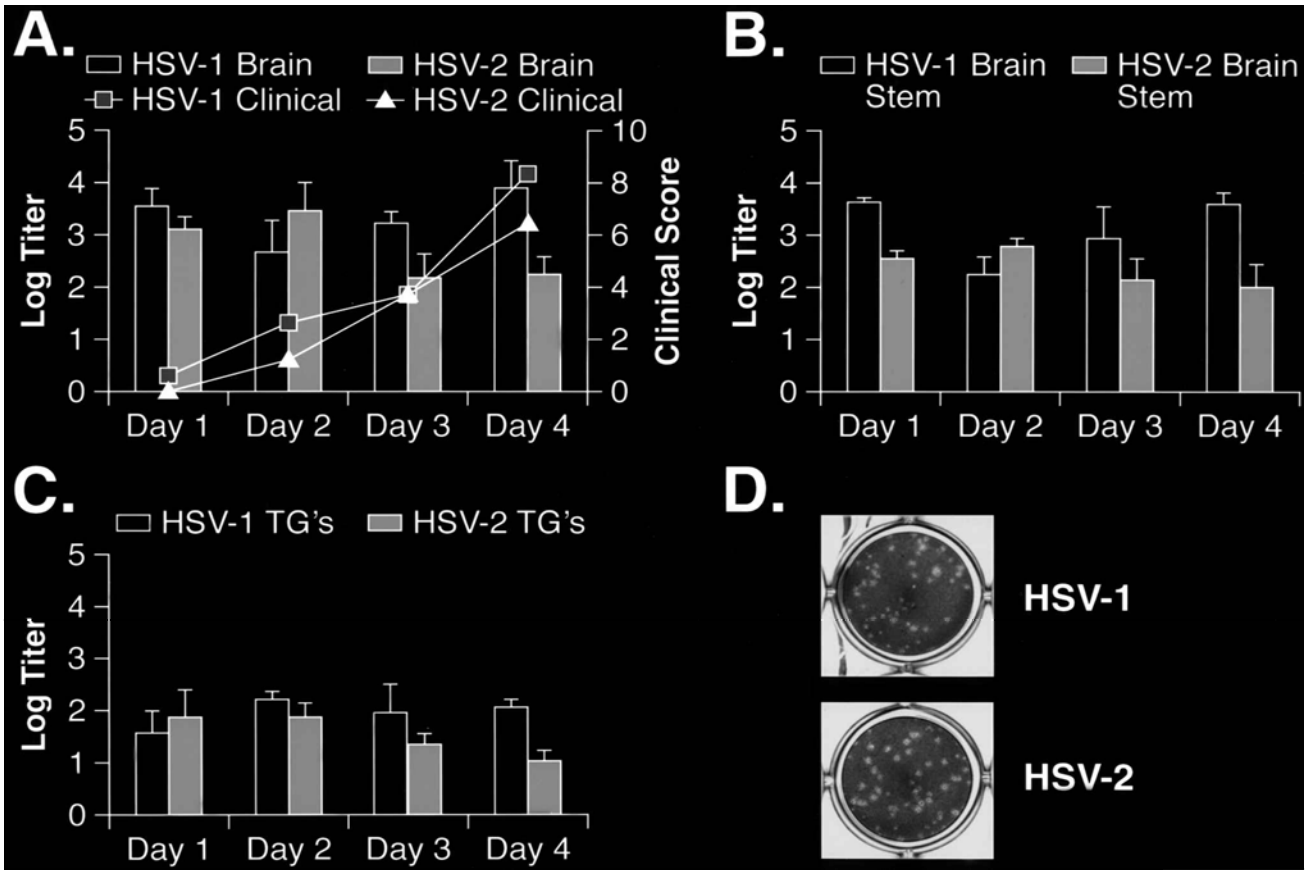

Figure 6 HSV-2 titers decrease by day 2 post-infection. BALB/c mice were infected with 1 μl (100 PFU) of HSV-1 (SC-16) or HSV-2 (SB-5). On days 1–4 postinfection, animals were observed clinically (**A**, lines, right axis) and titers were determined for brains (**A**, bars, left axis), brainstems (**B**), and trigeminal ganglia (**C**). Following inoculation, 1 μl was plated onto RSC monolayers to determine inoculating virus titer (**D**). Five mice were used for each time point.

In a time course experiment, HSV-1 and HSV-2 titers in brains, brain stems, and trigeminal ganglia were similar on days 1 and 2 following inoculation with 100 PFU per brain. However, marked reduction in HSV-2 titers was observed by days 3 and 4 (Figure 6A,B,C, bars). Therefore, by day 4 postinfection, HSV-2 replication is not as efficient as that of HSV-1. As observed in our previous experiment (Figure 5), both serotypes caused similar clinical disease (Figure 6A, lines) suggesting that the pathology was inflammation and not titer-dependent. Based on antigen and histological analysis, this drop in virus titer in HSV-2 infected samples may result from destruction of meningeal cells harboring virus. To evaluate if the differences observed did not result from inoculating titer variations or differences in the syringes used for inoculation, the amount of virus in 1-μl inoculum was confirmed by plaque assay. No differences were observed (Figure 6D).

Brain pathology induced by different HSV isolates

To determine whether the differences we observed between HSV serotypes were due to unique characteristics of HSV-2 (SB-5), we examined the clinical disease, brain lesions, and antigen distribution induced by other viral strains. The early passage HSV-1 (RS-1) and HSV-2 (RS-2, 3, 4) clinical isolates were obtained directly from genital swabs. We also compared HSV-2 (SB-5) to the laboratory passaged strain HSV-2 (MS). Mock-infected animals displayed no clinical disease, antigen staining, or histopathology. On day 4 postinoculum, only MS and SB-5 infected mice displayed clinical signs of infection. Animals inoculated with the clinical isolates began to display clinical signs and mortality on day 8 postinfection, consistent with a low titer inoculum. As expected, the HSV-1 clinical isolate RS-1 caused disseminated necrotizing encephalitis within the cerebral cortex, hippocampus (bilateral), thalamus, hypothalamus, and cerebellar brain stem (not shown). Similar to HSV-2 (SB-5), HSV-2 clinical isolates RS-2 and RS-3 caused meningitis and ventriculitis with minimal extension into the underlying parenchyma around the ventricular system (not shown). However, laboratory HSV-2 strain (MS) antigen and lesion distribution appeared to be a hybrid between HSV-1 (SC-16) and HSV-2

(SB-5). Although antigen expression was predominantly meningeal, there were numerous small foci of antigen-positive cells within the cerebellar brain stem, cerebellar molecular and granular layers, thalamus, hypothalamus, cerebral cortex, and hippocampus. In sections obtained from the clinical HSV-2 isolate RS-4 on day 8, there was disseminated distribution of antigen-positive cells within the cerebral cortex, hippocampus, thalamus, cerebellum, and brain stem, as well as the meninges (not shown). This correlated with severe necrotizing encephalitis and meningitis in areas that were antigen-positive. Thus, the clinical isolate RS-4 mimicked the pattern of dissemination and lesion formation seen with all isolates of HSV-1 that we examined, suggesting that the inoculum contained a mixed HSV-1 and HSV-2 population (Sucato *et al*, 1998).

Discussion

The utility of *in vivo* high-resolution magnetic resonance imaging for following brain pathology has been well demonstrated in several disease models in rats and mice (Sarkar and Kapadia, 1992). A recent study by S. Xu *et al* (1998) in the mouse experimental allergic encephalitis model demonstrated the ability to correlate 4.7 T MR with histopathology. We have carried out a systematic study to diagnose and understand the pathology induced by two pathogens, HSV-1 and HSV-2, using high-resolution MRI. The results were compared to standard histology to validate MR observations. These comparative studies are critical for validating whether MRI technology can be useful in carrying out routine longitudinal studies to evaluate virus-related pathology in mouse models. The experiments reported here demonstrate the utility of *in vivo* 4.7 T MRI for following the progression of brain damage in individual animals in this preclinical model of HSE. Our results suggest that brain pathology could be detected by high-resolution *in vivo* MRI as early as 2 days following infection with 1000 PFU of HSV-1. However, for mice infected with low dose (100 PFU) of HSV-1, administration of contrast agent was necessary to visualize the lesions. This result is consistent with earlier studies with contrast agent enhanced MRI (Meyding-Lamade *et al*, 1998a, b). We show an excellent correlation between the lesions observed by MRI in brains of HSV-1 infected animals to those observed by histopathology and immunohistochemistry. It is also demonstrated that the images obtained at higher magnetic field strength (9.4 T) of *ex vivo* brains from infected mice show anatomical details of the brain and the lesion. These findings correspond very well with the histological results (Figure 2).

We were unable to observe HSV-2-induced lesions that were identified by high magnification histology (Figure 4) using *in vivo* MRI at 4.7 T with the exception of one mouse (Table 2, B-11). Moreover, clinical disease in HSV-2 infected animals did not correlate with MR or histopathology. It is possibly due to the meningeal distribution of HSV-2 related inflammation. Meninges, even in control animals, displayed hyperintensity making interpretation difficult. These data suggest that MR is useful in detecting parenchymal but not meningeal lesions. In support of this interpretation, we consistently detected parenchymal inflammation caused by HSV-1 by MR, but not when HSV-1 induced only necrotizing meningitis. For example, in one HSV-1 infected animal (Table 2, B-5) histopathology was limited to multifocal moderate necrotizing meningitis and no lesions were detected by 4.7 T MRI. Thus, it is possible that similar to its indication in the clinic (Post *et al*, 1988), MRI may only be useful for evaluation of encephalitis with infiltration to the parenchyma and not for early stages of meningitis.

Several HSV-2 strains caused predominantly meningitis, whereas HSV-1 strains induced disseminated necrotizing meningoencephalitis, similar to observations in humans. In contrast to our findings (Table 2, Figure 4), several studies reported that intracranial infection with HSV-2 caused severe brain pathology and widely disseminated antigen distribution. For example, inoculation with HSV-2 strain MS at 15 PFU in 30 μl was lethal (62%) and brain virus titer on day 7 was 3000 PFU/brain. Antigen was detected in the hippocampus (pyrramidal neurons) and striatum but not in the cortex or thalamus (Gressens and Martin, 1994). A possible explanation is that we microinjected virus intracerebrally in a total volume 1 μl, whereas in the studies mentioned above inoculum volumes ranged from 15–30 μl. The differences in distribution may be due to back flow of the inoculum upon injection of larger volumes that caused widely distributed virus spread through the cerebrospinal fluid. Alternatively, differences in distribution and replication efficiency may be due to variation in inoculation sites (Kesari *et al*, 1996), mouse or viral strains.

We observed lower HSV-2 (SB-5) titers in the brain and trigeminal ganglia relative to HSV-1 (SC-16) (Figures 5 and 6). It is possible that HSV-2 spread, and not HSV-2 replication efficiency, is reduced relative to HSV-1, either due to the presence of fewer receptors for HSV-2 in neurons and glial cells (Vahlne *et al*, 1980) or to an altered immune response. Previous studies using high titer inocula demonstrated efficient replication of HSV-2 strains in mouse brains (Martin *et al*, 1982; Thompson and Stevens, 1983; Georgsson *et al*, 1987; Gressens *et al*, 1994). A direct comparison of replication kinetics in brains of mice inoculated with 10^6 PFU of HSV-1 (17 Syn+) or HSV-2 (HG-52) demonstrated that although virus titers were identical at 24 h postinfection, HSV-1 titers were over 1 log higher by 36 and 48 h p.i. (Thompson and Steven, 1983). These data are consistent with our

observations in mice infected with 100 PFU (Figures 5 and 6).

HSV-2 (SB-5) antigen distribution was limited to meningeal regions, occasionally to the underlying parenchyma, and the distribution or intensity was inconsistent with the high viral titers detected in the brains. In contrast, HSV-1 antigen was disseminated throughout the brain, consistent with high viral titers. It has been reported that viral nucleic acid could be detected by *in situ* PCR in more brain foci than predicted by immunostaining for viral antigen (Gressens *et al*, 1994). Therefore, it is possible that efficient HSV-2 replication is limited to meningeal cells and that in neuronal cells the production of HSV proteins is below detectable levels.

In this study, we observed the lack of parenchymal brain inflammation in HSV-2 infected animals. Our data are consistent with case studies of patients who succumbed to HSV-2 encephalitis (ascending myelitis) without histological evidence of brain inflammation (Tucker *et al*, 1985). In contrast to HSV-1, HSV-2 mediates intracellular sequestering of class II major histocompatability complex (MHC) antigens (Lewandowski *et al*, 1993). This limited antigen presentation in the CNS was previously associated with altered induction of IL-6 and IFN-gamma transcripts in response to infection (Lewandowski *et al*, 1994; Lewandowski *et al*, 1998; Lewandowski and Hobbs, 1998). Thus, an altered cytokine profile in the brains of HSV-2 infected individuals may result in reduced recruitment of inflammatory cells and differences observed by MRI and histopathology.

In conclusion, *in vivo* and *ex vivo* MR imaging provide an opportunity to evaluate brain lesions in individual animals over time as a complementary approach to histologic studies and may be useful for evaluation of the efficacy of anti-infective therapeutic approaches.

Materials and methods

Cells and virus

HSV-1 strain SC-16 (Hill *et al*, 1975), HSV-2 strain SB-5 (ATCC VR-2546, Sutton *et al*, manuscript in preparation), a plaque-purified early isolate of strain 333 (Galloway and Swain, 1980), and strain MS (ATCC VR-540) were grown on human MRC-5 cells (ATCC CCL-171). All stocks were titered on rabbit skin cells (Thompson and Stevens, 1983).

Mice

Female BALB/c AnNcrlBr (4–6 weeks old) were obtained from Charles River Laboratories (Raleigh, NC). All animal studies were approved by SmithKline Beecham Pharmaceuticals Institutional Animal Care and Use Committee.

Intracerebral inoculation

Mice were anesthetized by intraperitoneal injection of ketamine (40 mg/kg; Fort Dodge Labs, Fort Dodge, IA) and xylazine (5 mg/kg; Miles, Shawnee Mission, KS), and the heads were cleansed with 70% ethanol. Inoculation was modified from a method described previously (Kesari *et al*, 1996). Following a midline incision, the skull was perforated using a 27-gauge needle approximately 2 mm caudal of the bregma and 1 mm left of the midline. An appropriate amount of virus (10^2–10^4 PFU of virus in 1 μl) or vehicle (PBS containing 10% fetal calf serum) was injected using a 5-μl Hamilton syringe with a 32-gauge needle. The injection was performed over approximately 1 min. The needle was left in for 1 min after the injection, then withdrawn slowly, as described previously (Kesari *et al*, 1996). The superficial skin wound was closed with VetBond tissue adhesive or sutures, and the mice were inspected daily for signs of illness.

Clinical disease evaluation

The animals were observed daily by two independent observers and clinical scores ranging from 1–10 based on severity were documented. The two independent observers arrived at the same score throughout the study. Symptoms such as ruffled coat, eyes tightly shut ("squinting"), reduced body tone, and head tilt were scored as 1. Circling and lethargy (demonstrated by reduced response to stimuli) were scored as 1.5; hunched posture and wasting (cahexia) were scored as 2; and seizures, limb paralysis, or severe respiratory distress demonstrated by labored breathing were scored as 10. All mice with a cumulative score of 10 were euthanized immediately using carbon dioxide and brains were removed for analysis.

In vivo MRI

All *in vivo* MRI experiments were conducted on a Bruker Biospec MRI system (Billerica, MA) operating at a magnetic field strength of 4.7 Tesla. T_2 weighted images were collected using a 3.5-cm birdcage resonator with spin-echo imaging sequence with the following parameters: field of view (FOV) = 2.5 $\times$ 2.5 cm, matrix size = 256 $\times$ 256; echo time (TE)/repetition time (TR) = 30/1500 ms, number of experiments (NEX) = 4. Twelve slices, each 1-mm thick, of the mouse brain were collected with an in-plane resolution of 102 $\times$ 102 μm.

Contrast-enhanced in vivo MRI

Gadopentate-Dimeglumine (Berlex Laboratories, Wayne, NJ) was administered intravenously at 0.2 mmol/kg body weight. Identical parameters to those described previously were used with the exception of TE/TR = 30/800 ms.

Ex vivo MRI

Following *in vivo* MR, brains were removed and fixed as described later. MRI experiments were carried out on a 9.4 T Bruker spectrometer with micro-imaging accessories with the following parameters: images were obtained with 3-dimensional

spin-echo sequence with a TE (echo time) = 30 ms and TR (repetition time) = 500 ms. A field of view of 1.5 cm × 1.5 cm × 1.6 with a matrix size of 256 × 128 × 136 was utilized, resulting in a resolution of 58 × 117 × 117 μm. Two averages were acquired, resulting in a total scan time of 5 h per sample. Each sample was then embedded in paraffin blocks and evaluated histologically.

Tissue collection
At varying times postinfection, mice were euthanized with carbon dioxide and exsanguinated via the descending aorta. The following tissues were removed aseptically: brain, brain stem, spinal cord, liver, spleen, heart, lungs, trigeminal ganglia, kidneys, and cervical lymph nodes. For determination of virus titers, tissues were placed in culture media. For histological analysis, tissues were rinsed in ice-cold PBS, fixed for 24 h in 10% normal buffered formalin, and stored in 70% ethanol.

Virus titration
Tissues were homogenized and subjected to one freeze-thawing cycle. Cell debris was cleared by centrifugation and supernatants were serially diluted and added to rabbit skin cells in microtiter plates. Following 1 h adsorption at 37°C, monolayers were overlayed with methylcellulose. At 48 h postinfection, plates were stained with crystal violet and virus plaques were counted using an imaging system (Phase 3 Imaging Systems).

Immunohistochemistry for HSV antigen
Slides containing standard 5-μm sections of brain were deparaffinized, rehydrated, and placed in phosphate buffered saline (PBS) with 0.1% Tween 20. Sections were stained using a Streptavidin-HRP labeling system on the DAKO Autostainer (DAKO, Carpinteria, CA). Briefly, the sections were exposed to 3% hydrogen peroxide for 20 min followed by a protein block with normal goat serum at a dilution of 1:50. Next, the primary antibody, rabbit anti-HSV-1 (DAKO), was applied at a dilution of 1:500 for 45 min at room temperature followed by an anti-rabbit IgG biotinylated secondary antibody applied at a dilution of 1:200 (Vector Laboratories, Burlingame, CA) for 30 minutes. Slides were incubated in a 1:200 dilution of Streptavidin-HRP (DAKO) followed by 3'3'-diaminobenzidine (DAB). The slides were counterstained with hematoxylin, dehydrated, and coverslipped. Negative controls included omission of primary antibody as well as staining of mock-infected tissue sections.

HSV antigen grading
The degree of positive staining for HSV antigen within the brain was graded according to the following criteria: absent = 0, rare positive isolated cells = 1, occasional positive cells either isolated or in small foci = 2, frequent positive cells typically in larger foci = 3, multiple locally extensive areas of intensely positive cells = 4.

Histologic lesion severity score for H&E stained sections
Slides containing standard 5-μm sections of brain were deparaffinized, rehydrated, and stained with hematoxylin and eosin (H&E). The severity of HSV-induced lesions in mice brains were graded based on the following scoring system. The presence and severity of meningitis, encephalitis, and lateral ventricular dilation were assessed in H&E stained sections of brain from each animal. Each category was scored individually as described in Table 1.

Clinical virus isolates
Clinical virus samples were a generous gift from Robert T Sarisky (SmithKline Beecham Pharmaceuticals). All samples were primary isolates and had not been passaged in culture. Samples were obtained from genital swab material in DMEM with 10% serum. Three mice per virus sample were inoculated intracerebrally with 1-μl virus suspension, virus titers of inocula were determined by plaque assays on RSC cells, and the remainder was used to inoculate MRC-5 cells for preparation of virus stocks. Viral serotype was verified using Imagen HSV typing kit as suggested by manufacturer (DAKO). Titers of the clinical stock inocula were HSV-1 (RS-1) 10 PFU/1 μl; HSV-2 (RS-2) 0.715 PFU/1 μl; HSV-2 (RS-3) 0.21 PFU/1 μl; HSV-2 (RS-4) 31^1 PFU/1 μl.

Acknowledgements

We thank Joshua Levin, Latitia Floyd, Rosanna Mirabile, Kate Rhodes, and Thomas Covatta for excellent technical assistance and Connie Hunter for critical review of the manuscript.

References

Anderson JR, Field HJ (1983). The distribution of herpes simplex type 1 antigen in mouse central nervous system after different routes of inoculation. *J Neurol Sci* **60:** 181–195.

Bergstrom T, Vahlne A, Alestig K, Jeansson S, Forsgrenm, Lycke E (1990). Primary and recurrent herpes simplex virus type 2-induced meningitis. *J Infect Dis* **162:** 322–330.

Corey L, Spear PG (1986). Infections with herpes simplex viruses. *N Engl J Med* **314:** 686–691.

Craig CP, Nahmias AJ (1973). Different patterns of neurologic involvement with herpes simplex virus types 1 and 2: isolation of herpes simplex virus type 2 from the buffy coat of two adults with meningitis. *J Infect Dis* **127:** 365–372.

Day SP, Lausch RN, Oakes JE (1988). Evidence that the gene for herpes simplex virus type 1 DNA polymerase accounts for the capacity of an intertypic recombinant to spread from eye to central nervous system. *Virology* **163:** 166–173.

Galloway DA, Swain M (1980). Cloning of herpes simplex virus type 2 DNA fragments in a plasmid vector. *Gene* **11:** 253–257.

Georgsson G, Martin JR, Stoner GL, Webster HF (1987). Virus spread and initial pathological changes in the nervous system in genital herpes simplex virus type 2 infection in mice. A correlative immunohistochemical, light and electron microscopic study. *Acta Neuropathol* **72:** 377–388.

Gressens P, Langston C, Martin JR (1994). In situ PCR localization of herpes simplex virus DNA sequences in disseminated neonatal herpes encephalitis. *J Neuropathol Exper Neurol* **53:** 469–482.

Gressens P, Martin JR (1994). *In situ* polymerase chain reaction—Localization of HSV-2 DNA sequences in infections of the nervous system. *J Virol Methods* **46:** 61–83.

Hill TJ, Field HJ, Blyth WA (1975). Acute and recurrent infection with herpes simplex virus in the mouse: a model for studying latency and recurrent disease. *J Gen Virol* **28:** 341–353.

Kern ER, Richards JT, Glasgow LA, Overall JC Jr, de, Miranda P. (1982). Optimal treatment of herpes simplex virus encephalitis in mice with oral acyclovir. *Am J Med* **73:** 125–131.

Kesari S, Lasner TM, Balsara KR, Randazzo BP, Lee VM, Trojanowski JQ, Fraser NW (1998). A neuroattenuated ICP34.5-deficient herpes simplex virus type 1 replicates in ependymal cells of the murine central nervous system. *J. Gen Virol* **79:** 525–536.

Kesari S, Lee VM, Brown SM, Trojanowski JQ, Fraser NW (1996). Selective vulnerability of mouse CNS neurons to latent infection with a neuroattenuated herpes simplex virus-1. *J Neurosci* **16:** 5644–5653.

Levitz RE (1998) Herpes simplex encephalitis: a review. *Heart Lung* **27:** 209–212.

Lewandowski G, Hobbs MV (1998). Evidence for deficiencies in intracerebral cytokine production, adhesion molecule induction, and T cell recruitment in herpes simplex virus type-2 infected mice. *J Neuroimmunol* **81:** 58–65.

Lewandowski G, Hobbs MV, Bloom FE (1994). Alteration of intracerebral cytokine production in mice infected with herpes simplex virus types 1 and 2. *J Neuroimmunol* **55:** 23–34.

Lewandowski G, Hobbs M, Geller A (1998). Evidence that deficient IFN-gamma production is a biological basis of herpes simplex virus type-2 neurovirulence. *J Neuroimmunol* **81:** 66–75.

Lewandowski GA, Lo D, Bloom FE (1993). Interference with major histocompatibility complex class II-restricted antigen presentation in the brain by herpes simplex virus type 1: a possible mechanism of evasion of the immune response. *Proc Natl Acad Sci USA* **90:** 2005–2009.

Martin JR, Stoner GL, Webster HD (1982). Lethal encephalitis and non-lethal multifocal central nervous system demyelination in herpes simplex virus type 2 infections in mice. *Br J Exper Pathol* **63:** 651–666.

Meyding-Lamade U, Haas J, Lamade W, Stingele K, Kehm R, Fath A, Heinrich K, Hagenlocher BS, Wildemann B (1998a). Herpes simplex virus encephalitis—long term comparative study of viral load and the expression of immunologic nitric oxide synthase in mouse brain tissue. *Neurosci Lett* **244:** 9–12.

Meyding-Lamade U, Lamade W, Kehm R, Knopf KW, Hess T, Gosztonyi G, Degen O, Hacke W (1998b). Herpes simplex virus encephalitis—cranial magnetic resonance imaging and neuropathology in a mouse model. *Neurosci Lett* **248:** 13–16.

Meyding-Lamade U, Lamade W, Kehm R, Oberlinner C, Fath A, Wildemann B, Haas J, Hacke W (1999). Herpes simplex virus encephalitis: chronic progressive cerebral MRI changes despite good clinical recovery and low viral load—an experimental mouse study. *Eur J Neurol* **6:** 531–538.

Nahmias AJ, Whitley RJ, Visintine AN, Takei Y, Alford CA Jr (1982). Herpes simplex virus encephalitis: laboratory evaluations and their diagnostic significance. *J Infect Dis* **145:** 829–836.

Oakes JE, Gray WL, Lausch RN (1986). Herpes simplex virus type 1 DNA sequences which direct spread of virus from cornea to central nervous system. *Virology* **150:** 513–517.

Post MJ, Tate LG, Quencer RM, Hensley GT, Berger JR, Sheremata WA, Maul G (1988). CT, MR, and pathology in HIV encephalitis and meningitis. *AJR Am J Roentgenol* **151:** 373–380.

Sarkar SK, Kapadia RD (1992). Magnetic resonance imaging in drug discovery research. In: *Magnetic resonance microscopy*. Blumish B, Kuhn W (eds). Weinheim: VCH, pp 513–531.

Skoldenberg B (1996). Herpes simplex encephalitis. *Scand J Infect Dis Suppl* **100**, 8–13.

Sucato G, Wald A, Wakabayashi E, Vieira J, Corey L (1998). Evidence of latency and reactivation of both herpes simplex virus (HSV)-1 and HSV-2 in the genital region. *J Infect Dis* **177:** 1069–1072.

Thompson RL, Stevens JG (1983). Biological characterization of a herpes simplex virus intertypic recombinant which is completely and specifically non-neurovirulent. *Virology* **131:** 171–179.

Tucker T, Dix RD, Katzen C, Davis RL, Schmidley JW (1985). Cytomegalovirus and herpes simplex virus ascending myelitis in a patient with acquired immune deficiency syndrome. *Ann Neurol* **18:** 74–79.

Vahlne A, Svennerholm B, Sandberg M, Hamberger A, Lycke E (1980). Differences in attachment between herpes simplex type 1 and type 2 viruses to neurons and glial cells. *Infect Immun* **28:** 675–680.

Whitley RJ, Kimberlin DW, Roizman B (1998). Herpes simplex viruses. *Clin Infect Dis* **26:** 541–553.

Whitley RJ, Lakeman F (1995). Herpes simplex virus infections of the central nervous system: therapeutic and diagnostic considerations. *Clin Infect Dis* **20:** 414–420.

Xu S, Jordan EK, Li W, Yang Y, Chesnick SA, Webster HD, Brocke S, Quigley L, McFarland HF, Frank JA (1998). *in vivo* three-dimensional MR microscopy of mice with chronic relapsing experimental autoimmune encephalomyelitis after treatment with insulin- like growth factor-I. *AJNR Am J Neuroradiol* **19:** 653–658.

Yeung KC, Oakes JE, Lausch RN (1991). Differences in the capacity of two herpes simplex virus isolates to spread from eye to brain map to 1610 base pairs of DNA found in the gene for DNA polymerase. *Curr Eye Res* **10 Suppl:** 31–37.